Peptide coacervates as intracellular delivery vehicles for synergistic cancer photothermal- and chemo-therapies

Cite as: APL Bioeng. **9**, 036101 (2025); doi: 10.1063/5.0279643
Submitted: 7 May 2025 · Accepted: 10 June 2025 ·
Published Online: 7 July 2025

View Online Export Citation CrossMark

Congxi Huang,[1] Sushanth Gudlur,[1] Syed Maricar,[1] Zilin Chen,[1] Anastasia Shebanova,[1] Yue Sun,[1] Valentin Saliba,[2] Cheng Xu,[3] Yiming Zou,[4] Jianghong Zhang,[4] Souhir Boujday,[2] and Ali Miserez[1,5,a)]

AFFILIATIONS

[1]Centre for Sustainable Materials (SusMat), School of Materials Science and Engineering, Nanyang Technological University (NTU), 50 Nanyang Drive, Singapore 637553
[2]Laboratoire de Réactivité de Surface, Sorbonne Université, 4 Place Jussieu, Paris 75005, France
[3]School of Chemistry, Chemical Engineering and Biotechnology, Nanyang Technological University (NTU), 62 Nanyang Drive, Singapore 637459
[4]School of Materials Science and Engineering, Nanyang Technological University (NTU), 50 Nanyang Avenue, Singapore 639798
[5]School of Biological Sciences, Nanyang Technological University (NTU), 60 Nanyang Drive, Singapore 637551

[a)]**Author to whom correspondence should be addressed:** ali.miserez@ntu.edu.sg

ABSTRACT

Intracellular delivery of large molecular weight therapeutics poses a significant challenge in targeted cancer therapy, as conventional delivery vehicles often fail to achieve efficient cellular uptake and controlled release. This study presents a solution using GW26 coacervate microdroplets (CMs), a peptide-based system, as a dual-function platform that not only facilitates the controlled release of therapeutic cargos but also enhances cancer cell death through photothermal therapy (PTT). GW26 CMs exhibit high recruiting efficiency of photothermal (PT) materials—chlorin e6 (Ce6) and gold nanorods—with over 80% efficiency. These CMs demonstrate high cellular uptake in tumor cells, with 98% of CT26 colon carcinoma cells successfully internalizing Ce6-loaded CMs. Upon near-infrared laser irradiation, the PT materials generate localized heat within the therapeutic range for PTT, triggering coacervate disassembly, concomitant cargo release, and death of different human cancer cells, including cervical cancer cells HeLa, colon cancer cells HCT116, and colorectal adenocarcinoma cells HT29. The co-recruitment of the cytotoxic protein saporin enables synergistic PT and chemotherapeutic cancer treatments among all these cells, further enhancing the therapeutic effect, in some cases exhibiting a near-complete loss in cell viability. This approach combines efficient recruitment, controlled cargo release, and enhanced therapeutic efficacy, positioning GW26 CMs as a promising platform for multimodal cancer therapies.

INTRODUCTION

Delivering large molecular weight (MW) therapeutics into cells using conventional delivery systems, including lipid nanoparticles (LNPs) and inorganic nanoparticles, remains a significant challenge in targeted cancer therapy.[1,2] These challenges arise primarily from cellular membrane barriers that restrict cargo transport, leading to limited intracellular drug bioavailability and reduced therapeutic efficacy.[3,4] Even if the lipid bilayer can be crossed by the delivery vector, endosomal entrapment is another challenge that needs to be considered. For example, LNPs often remain entrapped in endosomal compartments where the cargos are degraded. Ionizable lipids are increasingly employed in LNP formulations to facilitate endosomal escape, which can, however, result in dose-dependent cytotoxicity.[5,6] Furthermore, LNP formulation requires multiple components and microfluidic technology, which adds complexity to the manufacturing process.[7] Hence, recent research is increasingly focused on developing delivery platforms that are readily taken up by cells while exhibiting superior intracellular drug accumulation, low cytotoxicity, and manufacturing simplicity, particularly for chemotherapeutics and biologics that require sustained intracellular activity to achieve their full therapeutic potential.[8]

Peptide-based coacervate microdroplets (CMs) represent a recently developed advanced delivery system that effectively addresses the challenges mentioned above.[9] These CMs recruit a wide range of therapeutic agents and efficiently enter cells by a mechanism akin to macropinocytosis and phagocytosis, making them highly effective as delivery vehicles.[10] Our group pioneered the use of these CMs for drug delivery by focusing on the HB*pep* family of peptides.[11] Inspired by the histidine-rich beak proteins of the Humboldt squid, HB*pep*s feature tandem repeats of the GHGxY sequence motif, where x represents a hydrophobic residue.[12] Through intermolecular π–π stacking of tyrosine side chains and hydrophobic interactions, these peptides undergo phase separation into CMs under physiological conditions, triggered by pH changes, while simultaneously recruiting cargos present in the coacervation buffer, a process that occurs within a few seconds.[13]

Among the HB*pep* family is GW26, a 26-residue peptide with five tandem repeats of GHGxY motifs and a terminal tryptophan (Trp), which has been a foundational peptide for various modifications aimed at encoding stimuli responsiveness to the CMs.[14] Originally developed as a versatile drug delivery system, GW26 has demonstrated high cargo recruitment efficiency and excellent delivery efficacy *in vitro*.[14,15] Subsequent studies have modified the GW26 sequence to improve drug delivery and cargo release kinetics by introducing redox-responsive moieties that allow for controlled disassembly and cargo release within the cytoplasm.[16] Despite these advancements, the application of GW26 in the context of thermal-triggered cargo release has not been fully explored. In this study, we hypothesized that increasing the temperature would weaken the inter- and intra-molecular interactions between GW26 molecules while simultaneously strengthening the mixing entropy that offsets phase separation. This combination of effects would likely lead to the disassembly of the CMs and the release of the recruited cargos into the cytoplasm.

Given its potential for thermally triggered cargo release, GW26 is well suited for integration with photothermal therapy (PTT), an emerging modality that exploits heat to induce cancer cell death.[17,18] PTT leverages the ability of specific materials to absorb light and convert it into heat, inducing localized hyperthermia to damage and kill cancerous cells. Photothermal (PT) materials that absorb in the near-infrared (NIR) window (650–900 nm for NIR-I or 1000–1700 nm for NIR-II) significantly improve the efficiency of PTT, since NIR light in this range penetrates deeper into tissues, allowing better targeting of tumors and cancerous cells.[19,20] Cancer cells are particularly susceptible to heat-induced apoptosis, making PTT a promising strategy for selective cancer cell targeting.[21] The efficacy of PTT depends on the properties of PT agents, such as their absorption in the NIR window, biocompatibility, and light-to-heat conversion efficiency. Chlorin e6 (Ce6), an FDA-approved photosensitizer, and gold nanorods (AuNRs), which exploit localized surface plasmon resonance (LSPR) for tunable optical properties, are well-characterized PT agents that fulfill these criteria.[22–26]

In this study, GW26 CMs were used as a delivery platform for Ce6 and AuNRs, with the goal of achieving dual functionality: controlled release of therapeutic cargos via heat-induced disassembly of the CMs and enhanced cancer cell death through PT effects (Scheme 1). Overall, the findings demonstrate that GW26 CMs serve as an enhanced delivery platform for small and large MW therapeutics, enabling both the controlled release of therapeutic cargos and the efficient use of PT materials for heat-induced cancer cell death. The co-recruitment of the cytotoxic protein saporin enables synergistic PT and chemotherapeutic cancer treatments, further enhancing the therapeutic effect. This approach not only represents a significant advancement in the development of multifunctional delivery systems but also establishes a robust foundation for more effective and targeted cancer therapies.

RESULTS AND DISCUSSION

Characterization of GW26 CMs and PT materials

GW26, a 26-residue peptide (MW 2782 Da, Fig. S1A), was confirmed to undergo phase separation within a pH range of 7.4–9.0, as evidenced by a marked increase in turbidity, measured as the absorbance at 600 nm [Fig. 1(a)]. This turbidity, confirmed by differential interference contrast (DIC) imaging, was attributed to the formation of micrometer-sized CMs rather than peptide aggregates [Fig. 1(b)]. Further characterization showed GW26 CM's ability to recruit small MW fluorescent molecules (Fig. S1B), with an average diameter of around 500 nm following phase separation (Fig. S1C) that was maintained for at least 90 min post-coacervation (Fig. S1D). To investigate the potential for heat-induced cargo release from GW26 CMs *in vitro*, a series of experiments were conducted assessing the release of cargo across a temperature range of 25–65 °C [Fig. 1(c), Supplementary Figs.

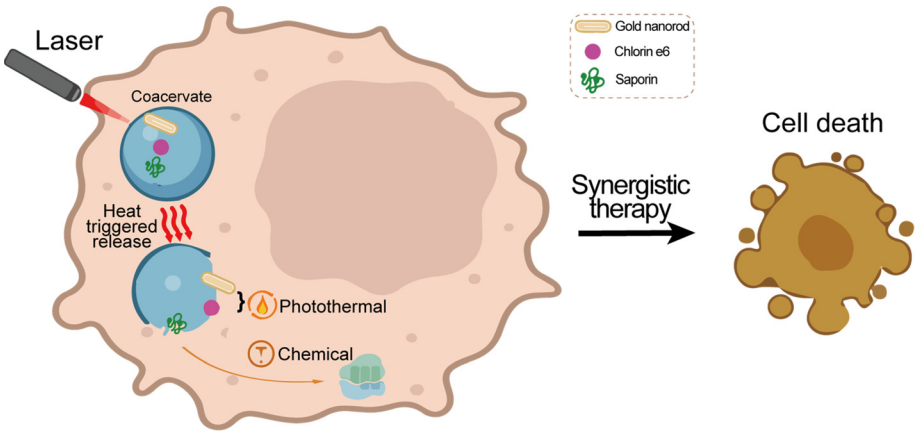

SCHEME 1. Schematic of GW26 CMs used as multifunctional delivery systems in cancer therapy. CMs recruiting PT materials and large MW cargos (here the cytotoxic protein saporin) are efficiently delivered into cancer cells. Upon NIR laser irradiation, PT materials generate localized heat, inducing coacervate disassembly and triggering the release of recruited cargos. The heat generated by PT materials directly induces cancer cell death, while the released cargos further enhance therapeutic efficacy through chemotherapeutic mechanisms, offering a synergistic approach to cancer treatment.

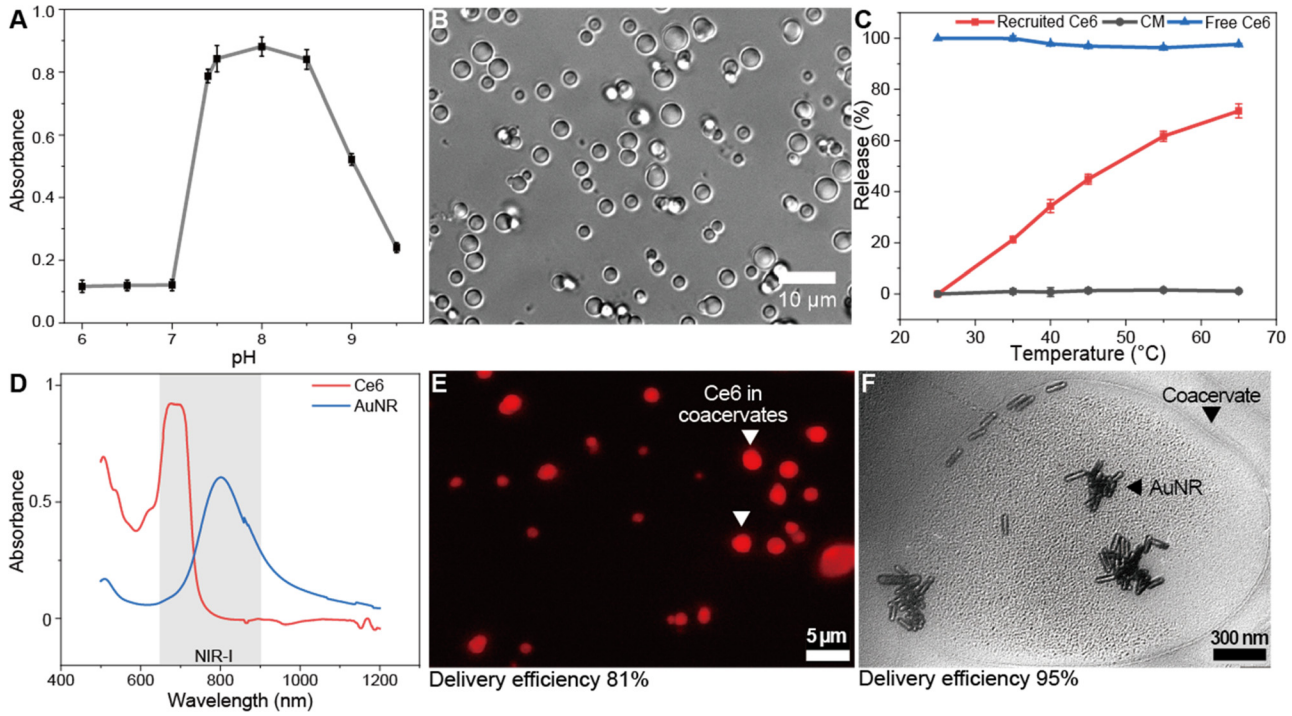

FIG. 1. Characterization of GW26 peptides, PT materials, and the recruitment of PT materials within GW26 CMs. (a) Turbidity measurements of GW26 peptides across a pH range of 6–10 confirm the peptide's narrow phase separation propensity within pH 7.4–9.0. (b) DIC image of a GW26 (0.33 mM) sample in Phosphate buffer saline (PBS) (pH 7.4) shows micrometer-sized peptide-dense CMs. (c) Fluorescence intensity measurements show a temperature-dependent increase in Ce6 release from GW26 CMs (red), reaching 50% at 45 °C and 70% at 65 °C. No significant change was observed in the controls: free Ce6 (blue) and GW26 CMs without Ce6 (black). (d) Absorbance spectra of Ce6 and AuNRs indicate peaks at ∼680 and ∼808 nm, respectively, both within the NIR-I window. (e) Fluorescence microscopy image of GW26 CMs loaded with Ce6 shows efficient recruitment of Ce6, as evidenced by the minimal background fluorescence outside the CMs. Triangle markers indicate Ce6 recruited within GW26 CMs. Recruitment efficiency is consistent with previously observed data for GW26.[14–16,28] (f) Representative TEM image of a single GW26 coacervate loaded with AuNRs indicates sparse recruitment of AuNRs within an intact coacervate. Triangle markers indicate AuNR or CMs.

S2A and S2B]. CMs were initially loaded with Ce6, one of the PT materials used in this study. Following centrifugation to sediment the CMs, it was observed that higher temperatures led to an increased concentration of Ce6 in the supernatant, indicating a temperature-dependent release mechanism. As shown in Fig. 1(c), the release of Ce6 after 10 min reached approximately 50% at 45 °C and increased to 70% at 65 °C, with no significant changes in the fluorescence intensity of the supernatant for the two controls: free Ce6 and GW26 CMs without Ce6. Since 45 °C is a typical target temperature for PTT, the time-dependent release of Ce6 at this temperature was further investigated. As shown in Supplementary Fig. S2B, Ce6 release was rapid and nearly linear during the first 10 min, followed by a slower rate of release that stabilized at around 80% after 60 min. Once heating was discontinued, the release gradually declined to around 10% over 50 min, demonstrating the CMs' capability to release the majority of their cargoes when heated to temperatures suitable for PTT. Dynamic light scattering (DLS) measurements further revealed that the size of the CMs decreased as the temperature increased, supporting the notion that coacervation was affected by temperature (Supplementary Fig. S2C). These findings establish the foundation for subsequent investigations into heat-triggered cargo release from GW26 CMs.

The PT materials used in this study included commercially obtained chlorin e6 (Ce6), a small molecule whose MW is 596.7 Da, with its chemical structure shown in Supplementary Fig. S3A and fluorescence excitation and emission peak shown in Fig. S3B, and gold nanorods (AuNRs), which were synthesized via a seed-mediated growth method (details provided in the Methods section). The resulting AuNRs were coated with silica to improve their biocompatibility and chemical stability.[27] Transmission electron microscopy (TEM) images and DLS analysis confirmed that the AuNRs had dimensions of 88 ± 6 nm in length and 22 ± 2 nm in width (Supplementary Figs. S3C and S3D). The UV–visible spectra of the free Ce6 and AuNRs revealed their characteristic absorption peaks within the NIR-I window, occurring at approximately 680 nm for Ce6 and 808 nm for AuNRs, consistent with previous reports [Fig. 1(d)].[23]

Recruitment of PT materials into GW26 CMs

The recruitment of PT materials into GW26 CMs was achieved by diluting the peptide stock solution (in 10 mM acetic acid, pH ∼3) into pH 7.4 buffer containing the respective PT materials. The pH change from ∼3 to 7.4 triggered peptide coacervation and the simultaneous recruitment of cargo present in the buffer. The successful recruitment of Ce6 and AuNRs, each separately, into the CMs was confirmed through fluorescence microscopy and TEM, respectively, with distinct fluorescence observed for Ce6 and electron-dense

structures for AuNRs within the CMs [Figs. 1(e) and 1(f)]. The recruitment efficiency was further quantified by measuring the concentration of PT materials in the supernatant of the samples with and without GW26 peptide after centrifugation. This analysis revealed that Ce6 and AuNRs were recruited with efficiencies of 81% and 95%, respectively, consistent with previously reported data for similar cargo types.[14–16,28]

Optimizing the peptide-to-cargo ratios was crucial for maximizing PT performance while minimizing the aggregation of PT materials during coacervation. A concentration of 50 μg/mL for Ce6 and AuNRs was identified as optimal, achieving a balance between strong PT response and coacervate stability [Figs. 1(e) and 1(f)]. Under this condition, most Ce6 could be recruited in the CMs, creating a highly concentrated internal environment. For AuNRs, TEM imaging revealed that at 50 μg/mL, they occupied only a small fraction of the coacervate volume, indicating sparse but effective recruitment without compromising coacervate structural integrity [Fig. 1 (f)]. These optimized conditions were used for all subsequent experiments unless otherwise noted.

Evaluating the PT activity of recruited PT materials

The conversion of absorbed NIR light into heat by PT agents like Ce6 and AuNRs relies on distinct mechanisms. For Ce6, upon NIR irradiation, the excited π-electrons in its tetrapyrrole backbone undergo non-radiative relaxation, releasing energy as heat.[29] AuNRs, on the other hand, leverage LSPR upon NIR exposure, which significantly enhances the electromagnetic field at their surface. This enhancement leads to the excitation of electrons, which then relax through non-radiative pathways, converting the absorbed energy into localized heat.[30]

To evaluate the PT performance of the recruited PT materials, Ce6- and AuNR-loaded GW26 CMs were exposed to laser irradiation at their respective peak absorbance wavelengths (680 nm for Ce6 and 808 nm for AuNRs) using an experimental setup as shown in Fig. 2(a), Supplementary Fig. S4A, and detailed in the Methods section. The temperature increase was monitored to assess the efficiency of light-to-heat conversion. Upon 5 min of laser irradiation, both Ce6 and AuNRs exhibited a significant increase in temperature. For Ce6-loaded CMs, the temperature increase ranged from 1.1 to 25.6 °C depending on the laser power density [Fig. 2(b)]. However, when the laser power density was held constant at 1 W/cm^2, the temperature increase varied by 7.0–9.5 °C when the recruited Ce6 concentration was varied from 25 to 100 μg/mL (Supplementary Fig. S4B), respectively. Notably, the recruitment of Ce6 into the CMs did not significantly alter its PT performance, as the increase in temperature was comparable to that of free Ce6 [Fig. 2(c)]. A similar pattern was observed for AuNR-loaded CMs, where the temperature increase varied from 1.7 to 14.8 °C depending on the laser power density [Fig. 2(d)]. However, when the laser power density was held constant at 1 W/cm^2, the temperature increase varied by 1.9–7.1 °C when the recruited AuNR concentration was varied from 12.5 to 50 μg/mL (Supplementary Fig. S4C). In contrast to Ce6, the PT performance of AuNRs was slightly affected by their recruitment within the CMs, as evidenced by a more modest increase in temperature of 7.6 °C compared to 15.6 °C for free AuNRs [Fig. 2(e)]. We hypothesize that the shift of the absorption peak when AuNRs are concentrated may be the underlying reason, as observed in previous research,[31,32] but this effect is minor for PT performance and PTT, as shown in the following experiments and detailed below.

Both Ce6- and AuNR-loaded CMs demonstrated excellent photostability, maintaining consistent PT performance across five cycles of laser-on-and-off tests (Supplementary Figs. S4D and S4E). The high photostability of the AuNRs is attributed to the silica coating, in agreement with previous reports.[27] The PT efficiency of the recruited materials, calculated from the cooling curves (detailed description in the Methods section), was found to be ∼50% for Ce6 and ∼48% for AuNRs [Fig. 2(f)], comparable to values reported in previous studies.[19] These results confirm that despite the microenvironment of the CMs, which might scatter some incident NIR light, the majority of the light penetrates and effectively triggers the PT effect. The system's ability to modulate temperature by adjusting laser power density or PT materials concentration makes it well suited for applications in PTT, where attaining a therapeutic temperature range of 40–45 °C is critical.

Delivery of recruited PT materials into cancer cells

The cellular delivery efficiency of PT materials, either AuNR- or Ce6-loaded GW26 CMs, was assessed first using the CT26 mouse colon carcinoma cell line, a common model in PTT studies.[33] Fluorescence microscopy revealed no detectable fluorescence signal in cells treated with free Ce6 [Figs. 3(a)–3(c)], indicating poor cellular uptake. In contrast, Ce6-loaded CMs successfully delivered Ce6 into the cells, as evidenced by a strong intracellular fluorescence signal from cells 1 day post-delivery [Figs. 3(d)–3(f)]. Fluorescence-activated cell sorting (FACS) analysis further confirmed a high delivery efficiency of Ce6, with 98% of the cells showing successful uptake of Ce6-loaded CMs, compared to only 5% uptake of free Ce6 [Fig. 3(g)].

Similarly, DIC microscopy images demonstrated the successful internalization of AuNR-loaded CMs, visible as dark particles within the cells [Figs. 3(h) and 3(i)]. Since AuNRs are not fluorescent, uptake quantification of AuNR-loaded CMs cannot be obtained by flow cytometry. Therefore, as an indirect method, we measured AuNR concentration in the media post-delivery and found that at least 75% of AuNR-loaded CMs were no longer in the media [Fig. 3(j)]. These results are consistent with previous studies on HB*pep* peptides and highlight the effectiveness of GW26 CMs as a delivery system for both Ce6 and AuNRs.[10,16,28]

Importantly, both the CMs and the PT materials exhibited minimal cytotoxicity in the absence of laser irradiation (Supplementary Fig. S5). Cell viability remained high—over 90%—3 days post-delivery for all experimental groups, including those treated with empty CMs and those loaded with PT materials (Supplementary Fig. S6A). These findings underscore the biocompatibility of the GW26 CMs and their safety as delivery vehicles for PT materials in cancer therapy.

PT performance of recruited PT materials *in vitro*

The PT performance of Ce6- and AuNR-loaded GW26 CMs was evaluated *in vitro* by assessing cell viability using the MTT assay following laser irradiation. Both PT materials exert their effects through localized hyperthermia, disrupting cellular integrity by denaturing proteins, damaging membranes, and triggering cell death.[21] Ce6 also generates reactive oxygen species (ROS) upon light exposure, adding an oxidative stress component that further amplifies cell death.[34] As a control, CT26 cells that were not treated with PT materials were

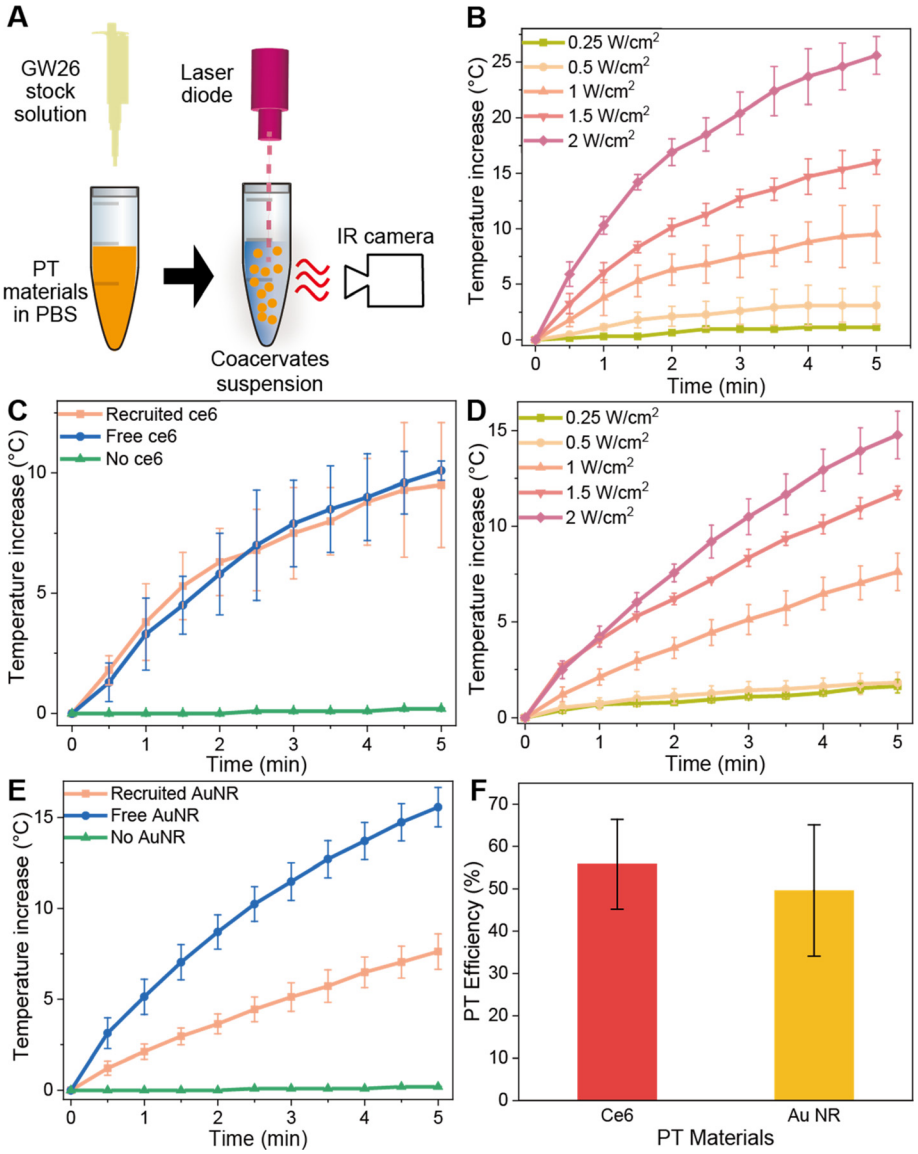

FIG. 2. PT performance of recruited PT materials in GW26 CMs. (a) Experimental setup: CM suspension was prepared by diluting the peptide stock solution into a buffer containing PT materials. The laser diode was positioned above the recruited PT materials in an Eppendorf tube, while an IR camera recorded the temperature of the CM suspension. (b) Temperature increase in Ce6-loaded GW26 CMs (initial concentration of Ce6 50 μg/mL) after 5 min of 680 nm laser irradiation at different power densities. (c) Comparison of temperature increase in Ce6-loaded GW26 CMs (initial concentration of Ce6 50 μg/mL), free Ce6, and PBS after 5 min of 1 W/cm^2 laser irradiation. (d) Temperature increase in AuNR-loaded GW26 CMs (initial concentration of AuNR 50 μg/mL) after 5 min of 808 nm laser irradiation at different power densities. (e) Comparison of temperature increase in AuNR-loaded GW26 CMs (initial concentration of AuNR 50 μg/mL), free AuNR, and PBS after 5 min of 1 W/cm^2 laser irradiation. Recruitment within CMs affects the PT performance of AuNRs, yet the temperature increase remains within the effective range for PTT. (f) PT efficiency of Ce6- and AuNR-loaded GW26 CMs.

exposed to laser irradiation. No significant reduction in cell viability was observed when the laser power density was kept below 1 W/cm^2 or the treatment time was less than 10 min. This established a baseline for subsequent experiments [Fig. 4(a), Supplementary Fig. S6B].

Laser irradiation (0.25–1.5 W/cm^2 for 5 min) of CT26 cells treated with PT material-loaded CMs resulted in a marked reduction in cell viability compared to control cells, indicating effective PT-induced cell death [Fig. 4(b)]. Cells treated with Ce6-loaded GW26 CMs showed a significant decrease in viability, dropping to 44% (0.6 W/cm^2) compared to approximately 78% for non-irradiated controls or cells treated with free Ce6 [Fig. 4(b), column 4 from left]. The extent of cell death could be modulated by adjusting the laser power density or concentration of Ce6, with higher power densities or Ce6 concentrations leading to greater reductions in cell viability [Fig. 4(c), Supplementary Fig. S6C].

For AuNR-loaded CMs, the PT effect was even more pronounced, with cell viability decreasing to 12% post-irradiation (1.5 W/cm^2 for 5 min), compared to nearly 90% in the absence of laser treatment [Fig. 4(b), column 2 from left; Fig. 4(d); and Supplementary Fig. S6D). This robust response underscores the superior PT performance of AuNRs, which, despite their slightly reduced efficacy when recruited, still outperformed free AuNRs in inducing cell death under controlled conditions, possibly by achieving higher temperatures at their surfaces when exposed to laser.[35]

To confirm cell death, CT26 cells were incubated with the fluorescent dye Hoechst 33342 and examined by fluorescence microscopy. As shown in Fig. 4(e), cells treated with both Ce6- and AuNR-loaded GW26 CMs exhibited significantly brighter fluorescence (indicative of cell death) after laser treatment compared to control cells that were not treated with the PT material-loaded CMs.

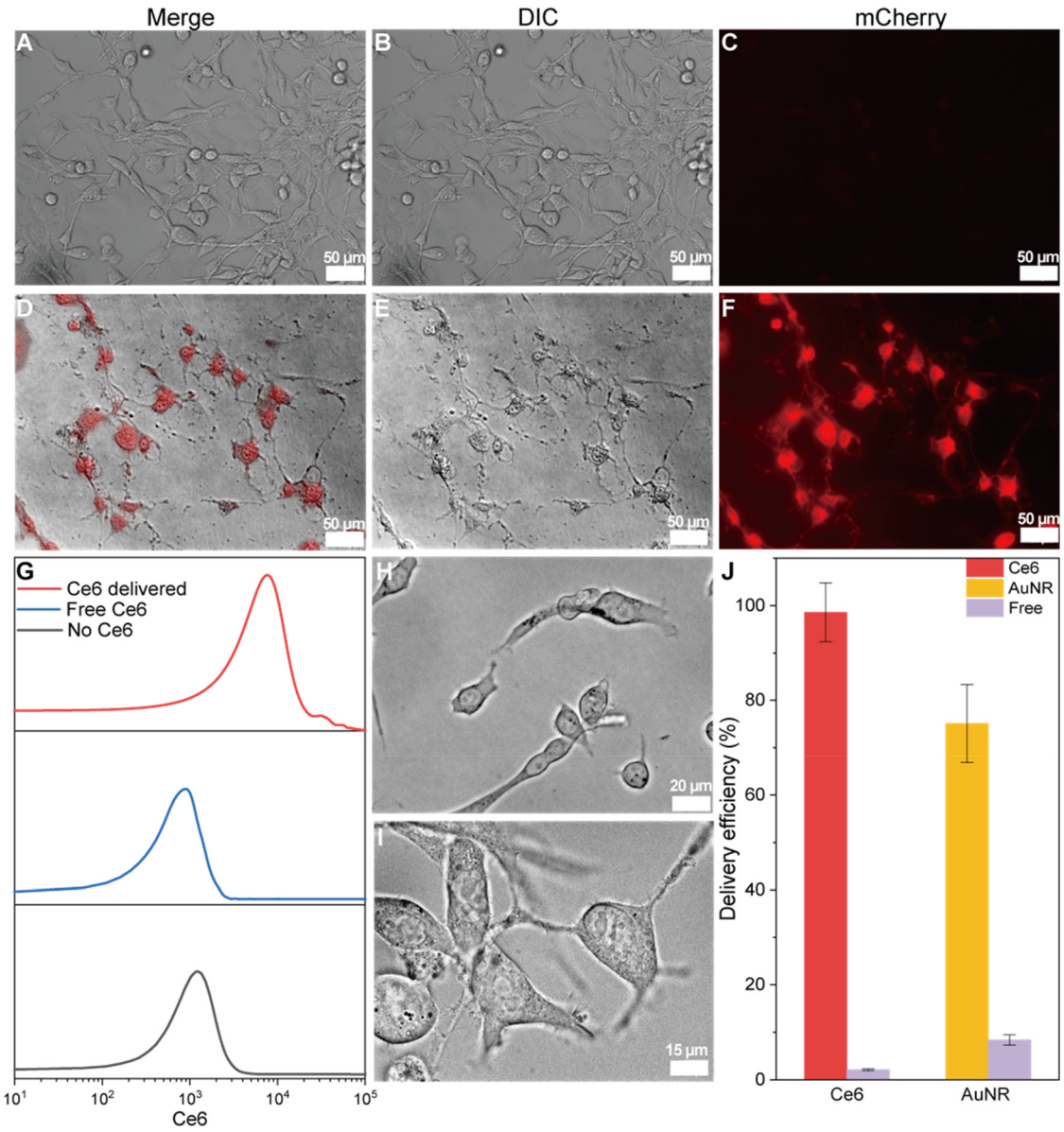

FIG. 3. Delivery of recruited PT materials into CT26 cells. (a) Merged image of (b) DIC image and (c) fluorescence image, showing control cells 1 day post-delivery of free Ce6. (a)–(c) No detectable uptake of Ce6. (d) Merged image of (e) DIC image and (f) fluorescence image, showing cells 1 day post-delivery of Ce6-loaded GW26 CMs. (d)–(f) Efficient uptake of Ce6, evidenced by the bright fluorescence within the cells, confirming that Ce6 requires a delivery system such as GW26 for effective cellular delivery. (g) Fluorescence signal of cells treated with free Ce6 or Ce6-loaded GW26 CMs, as measured by FACS, shows that nearly all cells have taken up Ce6 when delivered with GW26 CMs. (h) DIC image of control cells 1 day post-delivery of free AuNR showing few dark particles, indicating poor uptake. (i) DIC image of cells 1 day post-delivery of AuNR-loaded GW26 CMs showing a significant amount of dark particles, indicating enhanced AuNR uptake. (j) Delivery efficiency of Ce6 (measured by FACS) and AuNR (measured by quantifying residual AuNR) mediated by GW26 CMs highlights the significant enhancement in PT material uptake when delivered with GW26 CMs. The high delivery efficiency is consistent with previous studies.[10,16,28]

Synergistic PT- and chemo-therapy with saporin

Characterization of GW26 CMs and PT materials PT performance and synergistic therapy *in vitro* confirmed that GW26 CMs could release their cargos upon heat stimulation. Since the recruited PT materials generated significant heat upon laser irradiation, we hypothesize that this temperature increase could trigger CM disassembly while simultaneously releasing co-recruited cargos *in vitro*. Saporin, a ribosome-inactivating protein that leads to cell death via apoptosis,[36] is commonly used in cancer therapy and was chosen as the co-recruited cargo for these experiments. To test this hypothesis, saporin and PT materials were co-recruited within GW26 CMs, delivered into cells, and subjected to laser irradiation to assess whether cell viability would decrease further.

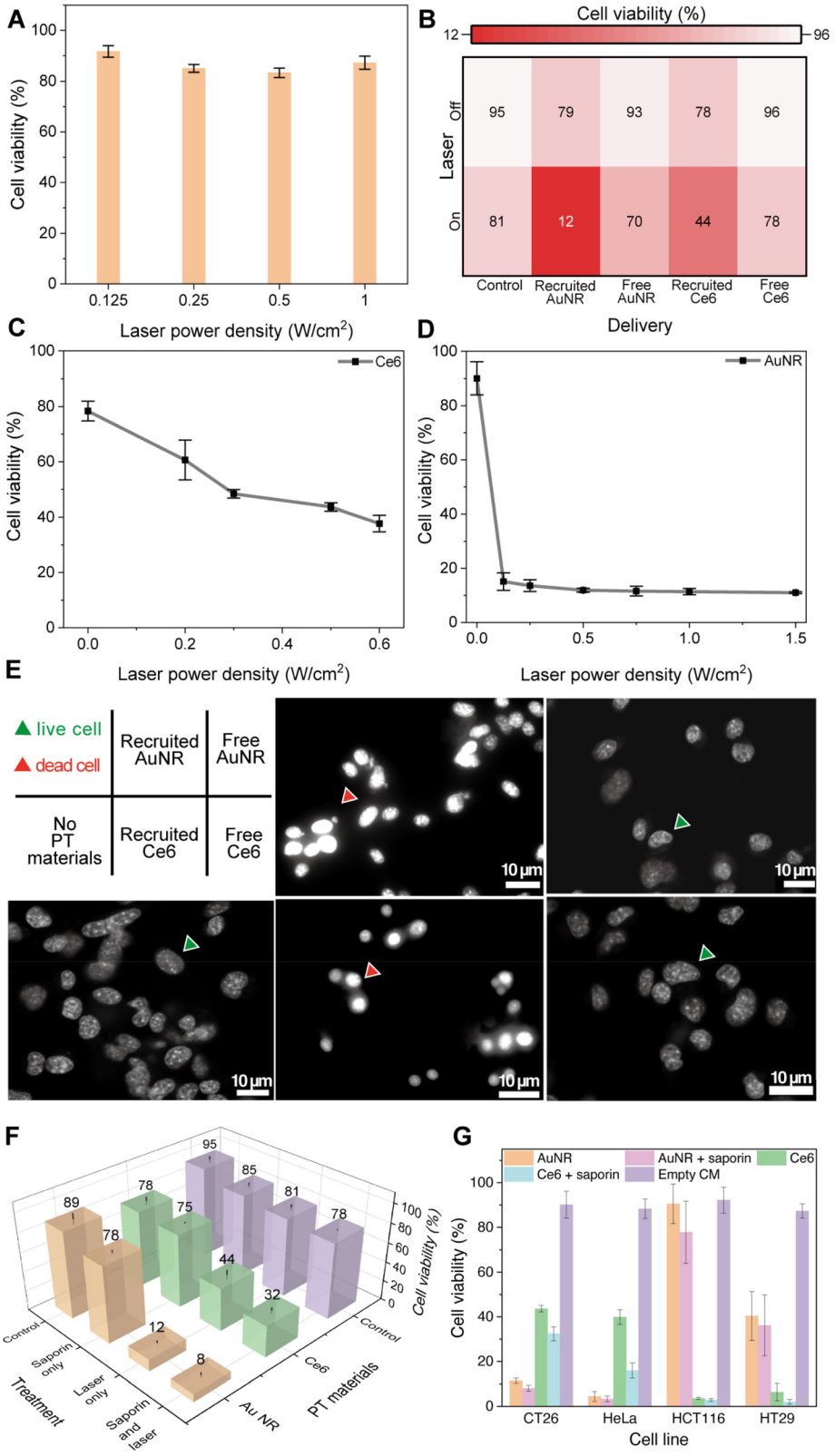

FIG. 4. Synergistic anti-cancer performance of PT materials and saporin mediated by GW26 CMs delivery *in vitro*. (a) Viability of cells in the absence of GW26 CMs or PT materials (50 μg/mL) and after 5 min irradiation of laser (1 W/cm^2) with different power densities shows no significant detrimental effect due to laser irradiation. (b) Cell viability under different combinations of laser, GW26 CMs-mediated delivery, or PT materials treatment. When the laser was applied to cells treated with PT material-loaded GW26 CMs, the viability significantly decreased. (c) Cell viability after incubation with Ce6-loaded GW26 CMs (50 μg/mL of Ce6) and 5 min of 0.2–0.6 W/cm^2 laser irradiation at different power densities. (d) Recruited 50 μg/mL AuNR treated cell viability after 5 min irradiation of 0.2–1.5 W/cm^2 laser with different power densities. (e) Hoechst 33342-dyed cells after 1 W/cm^2 laser irradiation for 5 min. The green triangles indicate live cells with dimmer fluorescence, while the red triangles indicate dead cells with brighter fluorescence. Cells treated with PT material-loaded GW26 CMs showed brighter fluorescence, implying lower viability. (f) Cell viability under different combinations of laser (1 W/cm^2), saporin, or PT materials treatment. Viability decreased further when laser was applied to cells for 5 min with both PT materials and saporin delivered. (g) Cell viability of different cell lines following GW26 CM-mediated delivery and laser irradiation (1 W/cm^2 for 5 min). All cell lines showed a decrease in cell viability after delivery of PT materials and laser irradiation, except HCT116 cells treated with AuNRs. A further decrease in viability was observed when the PT materials were co-recruited with saporin for all groups.

Upon laser irradiation, cell viability of CT26 cells reduced further compared to what was observed with only PT material-loaded GW26 CMs, which can be attributed to the release of saporin, triggered by heat-induced disassembly of CMs by the PT materials [Fig. 4(f)]. Specifically, cells treated with GW26 CMs co-recruiting AuNR and saporin exhibited a viability of just 8%, compared to 12% for cells treated with AuNR alone. Similarly, CT26 cells treated with GW26 CMs co-recruiting Ce6 and saporin showed a decrease in viability to 32%, compared to 44% for cells treated with Ce6 alone [Fig. 4(f)]. Notably, in the absence of laser irradiation, cell viability remained above 80% for all groups, confirming that the observed effects were due to the controlled release of saporin, triggered by NIR laser-induced heat.

A similar trend of reduced cell viability was observed in other human cancer cell lines, such as HeLa (human cervical cancer), HCT116 (human colon cancer), and HT29 (human colorectal adenocarcinoma). Following the treatment with GW26 CMs loaded with PT materials with/without saporin and under laser irradiation, these different cell types exhibited a significant reduction in cell viability when compared to control cells treated with the PT materials without GW26 CMs. Moreover, co-recruitment of saporin with either AuNR or Ce6 led to a slightly greater reduction in viability than PT materials alone. Notably, HeLa cells were highly sensitive to AuNR–saporin treatment, with viability dropping to ∼5%, while HCT116 cells exhibited near-complete loss of viability (∼2%) following treatment with Ce6–saporin.

Interestingly, CT26 and HeLa cells showed higher responsiveness to AuNR-mediated PTT, whereas HCT116 and HT29 cells were more susceptible to Ce6-mediated PTT. In contrast, HCT116 cells exhibited near-complete resistance to AuNR-based treatment. Although the mechanisms driving these cell-type-specific responses remain unclear, such variability has been previously reported. Varvarà *et al.* showed that AuNRs coated with lipoic acid and gellan gum elicited only modest PT effects in HCT116 cells, reducing viability by just 20%–40%.[37] The results suggest that mere thermal elevation alone may be insufficient to cause significant cytotoxicity in this cell line, although the underlying mechanisms were not further investigated. These cell line-dependent differences in PTT responsiveness likely reflect the broader phenomenon of therapeutic resistance, which is well documented in the context of both PT and photodynamic therapies.[38,39] Multiple factors may contribute to such resistance, including: (1) enhanced efflux of PT agents via ATP-binding cassette (ABC) transporters like P-glycoprotein (P-gp) and ABCG2; (2) activation of pathways that repair and tolerate PTT-induced damage; (3) upregulation of antiapoptotic proteins; (4) PTT-induced autophagy as a cue to promote cell growth; (5) nitric oxide (NO)-induced cryoprotective effects; (6) increased expression of heat shock proteins (HSPs); (7) activation of DNA repair mechanisms; and (8) changes in cytoskeleton, cell adhesion, and cell morphology. The exact reason for the difference of PT response in this research requires, thus, more extensive studies.

Despite differences in the magnitude of PTT-induced effects across cell types, these findings highlight the potential of GW26 CMs as an effective platform for combinatorial cancer therapies, where the synergistic effects of PTT and heat-triggered release of cytotoxic agents can be harnessed to achieve enhanced therapeutic outcomes.

CONCLUSION

This study demonstrates the versatility and efficacy of GW26 CMs as a robust platform for the delivery of PT materials, enabling both laser-induced heat-triggered cargo release and synergistic PTT. GW26 CMs were shown to efficiently recruit and deliver Ce6 and AuNRs into multiple cancer cell lines, with high recruitment efficiency and minimal cytotoxicity in the absence of external triggers. PT performance remained effective even after recruitment within the CMs, as evidenced by significant temperature increase upon laser irradiation, leading to effective cancer cell ablation.

Moreover, the potential for synergistic cancer therapies was explored by co-recruiting the cytotoxic protein saporin alongside PT materials within the CMs. The heat generated by laser-activated PT materials facilitated the controlled release of saporin, further enhancing the therapeutic effect and leading to significant reductions in cell viability. This dual-function approach of combining the cytotoxic effects of PTT with the controlled release of therapeutic agents demonstrates the potential of GW26 CMs to achieve more effective cancer treatments.

In summary, the findings extend the application of HB*pep* (GW26) CMs beyond simple drug delivery, positioning them as a versatile tool for intracellular delivery of PT materials and the facilitation of synergistic cancer therapies. The ability to finely tune the PT effect and control the release of therapeutic agents within the cellular environment underscores the potential of this system for future developments in combinatorial cancer therapies. Further research will focus on optimizing these CMs for *in vivo* applications, exploring their utility in a broader range of therapeutic contexts, and investigating the underlying cause of the observed variability in PT response.

METHODS

Materials

Wang resin ([4-[(4-methylphenyl)methoxy]phenyl]methanol) and fluorenylmethoxycarbonyl (Fmoc)-protected peptides were purchased from GL Biochem (Shanghai) Ltd. DMF (N,N-dimethylformamide), piperidine, oxyma (ethyl 2-cyano-2-(hydroxyimino)acetate), TIPS (triisopropylsilane), ACN (acetonitrile), α-CHCA (alpha-cyano-4-hydroxycinnamic acid), DMSO (dimethyl sulfoxide), $NaBH_4$ (sodium borohydride), NaOH (sodium hydroxide), CTAB (cetyltrimethylammonium bromide), MPTMS [(3-mercaptopropyl)trimethoxysilane], and TEOS (tetraethyl orthosilicate) were purchased from Sigma-Aldrich, Merck KGaA. DIC (N,N-diisopropylcarbodiimide), TFA (trifluoroacetic acid), and NaOL (sodium oleate) were purchased from Tokyo Chemical Industry Ltd. Diethyl ether and acetic acid were purchased from Schedelco Pte Ltd. DCM (dichloromethane), PBS, cell lines, DMEM, RPMI 1640, McCoy's 5A, FBS (fetal bovine serum), trypsin, EDTA (ethylenediaminetetraacetic acid), MTT [3-(4,5-dimethylthiazol-2-yl)-2,5-diphenyltetrazolium bromide], Hoechst 33342, and saporin were purchased from Thermo Fisher Scientific Inc. Ce6 was purchased from Adooq Bioscience Ltd. $HAuCl_4{\cdot}3H_2O$ (hydrogen tetrachloroaurate (III) trihydrate) was purchased from Alfa Aesar. $AgNO_3$ (silver nitrate) and ascorbic acid were purchased from Honeywell, Fluka. Hydrochloric acid was purchased from VWR Chemicals.

Synthesis and characterization of peptides

Peptides were synthesized using the solid-phase peptide synthesis method on an automated peptide synthesizer (LibertyBlue, CEM Corp.). Using Wang resin as a support, 5 mL piperidine (20 vol% in DMF) was added into the reaction vessel each time and reacted at

70 °C for 2 min to remove the protection group at the N-terminus of the peptide chain. Then, 5 mL N-terminus Fmoc-protected amino acids (2 M in DMF) was added into the reaction vessel each time, with 1 mL DIC (1 M in DMF), 1 mL oxyma (0.5 M in DMF), and 2 mL DMF. The reaction was performed at 90 °C for 4 min to couple the new amino acid to the peptide chain. The two steps were repeated until all amino acids were coupled. After synthesis was completed, the resin was transferred into a funnel and washed with DMF and DCM for 30–60 s with nitrogen bubbling. After dried by nitrogen flow, 5 mL cleavage cocktail was added to immerse the resin, including 95% TFA, 2.5% TIPS, and 2.5% H_2O. After cleaving for 2 h, the liquid phase was filtered. Then 30 mL cold diethyl ether was added, precipitating the peptides from the cleavage cocktail. The mixture underwent centrifugation at 8000 rpm, 10 min for three times to collect the peptides and wash the impurities on their surface. After centrifugation, the peptides were dried in nitrogen flow before being dissolved in 5% acetic acid. High-performance liquid chromatography (HPLC) was used to purify the peptides on an Agilent 1260 Preparative HPLC equipment with an Agilent C8 column. The mobile phase was water and ACN. After collection, the fractions containing peptides were transferred into a −80 °C refrigerator (Thermo Fisher Scientific Inc.). After freezing for 12 h, they were transferred into a freeze dryer (Labconco Corp.). Dry peptide samples were obtained after the freeze-drying finished in 1–2 days. The peptides were stored at −20 °C and dissolved in 10 mM acetic acid as a 10 mg/mL stock solution before usage.

As for the characterization of peptides, matrix-assisted laser desorption ionization—time of flight mass spectrometry (MALDI-TOF MS, Shimadzu Performance, Shimadzu Corp.) was used to detect the MW, with α-CHCA as the matrix. After confirming the peptide MW, the coacervation ability of the peptide was tested by measuring its turbidity on a plate reader (Tecan Spark, Tecan Trading AG). 20 μL GW26 peptide stock solution was pipetted into 180 μL buffers (Tris, phosphate, or Bis) with final pHs of 6.5, 7.0, 7.4, 7.5, 8.0, 8.5, 9.0, and 9.5, separately. The samples were then transferred into a 96-well plate, which was then inserted into the plate reader. Their absorbance at 600 nm was measured and compared. The absorbance represented the turbidity of the solution. Following turbidity measurements, 20 μL CM suspension diluted to 100 μg/mL in PBS was pipetted to a glass-bottom dish, and an optical microscope (Zeiss Life Cell Observer II, Leica Camera AG) was used to observe the morphology of the sample to confirm the coacervation in DIC using a 40× objective.

As for characterizing the release of cargoes from CMs when temperature increases, 0.1 mg Ce6 was dissolved in 1 mL PBS, and the peptide solution at the concentration of 2 mg/mL (in 10 mM acetic acid) was pipetted into the solution with a 1:9 (v/v) ratio. The CM suspension was then pipetted into 1.5 mL Eppendorf tubes for 1 mL each and centrifuged at 1000 rpm for 2 min to precipitate all CMs at the bottom. 100 μL supernatant from each tube was collected for measurement of fluorescence emission intensity later. All tubes were then sealed with Parafilm and put on a heating block (Hangzhou Xinyi Co. Ltd.), whose temperature was adjusted from 25 to 65 °C at a step of 10 °C. After the temperature reached each value and was maintained for 10 min, one Eppendorf tube was taken out, quickly centrifuged (4000 rpm, 10 s), and its top 100 μL supernatant was then collected and transferred into a 96-well plate. After all samples were collected and cooled to room temperature, the 96-well plate was inserted into the plate reader. Their fluorescence emission at 680 nm under excitation at 505 nm was measured and compared. Alternatively, the temperature of the heating block was maintained at 45 °C, and one Eppendorf tube was taken out every 10 min for sample collection. The release percentage r of the samples was calculated by

$$r = \frac{I_2 - I_1}{I_0 - I_1}, \tag{1}$$

where I_0 represents the fluorescence emission intensity of the samples before coacervation, I_1 represents the intensity of the supernatant after coacervation but before heating, and I_2 represents the intensity of the supernatant after heating.

DLS analysis was performed on a DLS analyzer (Zetasizer Pro, Malvern Panalytical Ltd). 200 μL CM suspension diluted to 50 μg/mL in PBS was pipetted into a quartz cuvette and inserted into the equipment. The size distribution and average size (calculated from the intensity distribution) were measured to quantify the variation of CM size for 90 min at 25 °C, and when the temperature rose from 25 to 65 °C (measured 10 min after the temperature stabilized).

Synthesis and characterization of PT materials

Ce6 was purchased commercially. AuNR was synthesized by the seed-mediated growth method. The seed solution was prepared by first mixing 5 mL of 200 mM of CTAB with 5 mL of 0.5 mM $HAuCl_4{\cdot}3H_2O$ dispersed in aqueous solutions at 30 °C and stirred at 700 rpm. 0.6 mL of freshly prepared $NaBH_4$ solution was then added to the $HAuCl_4{\cdot}3H_2O$–CTAB solution under vigorous agitation (1200 rpm) for 2 min to form the gold seeds, and the solution was matured for 30 min at 30 °C. The growth solution was prepared by mixing 7 g of 77 mM CTAB and 1.115 g of 15 mM NaOL in 250 mL of hot water first. Then, 24 mL of 4 mM $AgNO_3$ were added to the solution at 30 °C without stirring for 15 min. Next, 250 mL of 1 mM $HAuCl_4{\cdot}3H_2O$ aqueous solution, preheated to 30 °C, was added to the previous solution and allowed to react at 700 rpm for 90 min. Subsequently, 1.5 mL of 37 wt.% HCl was added to lower the pH to 1.8, with stirring maintained at 400 rpm for another 15 min. Then, 1.25 mL of a 64 mM ascorbic acid aqueous solution was added, and the solution was briefly stirred at 1000 rpm for 30 s. Finally, 400 μL of the preheated seed solution was injected into the above solution under vigorous stirring (1000 rpm) for another 30 s. The final suspension was aged undisturbed overnight in the oven at 30 °C. The next day, it was centrifuged at 7000 rpm for 30 min two times to remove the excess co-surfactants. To form silica coating, 3.8 mL of the stock 30 °C AuNR solution was centrifuged at 5600 rcf for 15 min, then 500 μL of the pellet was redispersed in 6.25 mL of water to set the CTAB concentration at 1.6 mM, followed by adjusting the pH to 4 and stirred at 400 rpm for 20 min. TEOS (20 vol% in MeOH) was then added to the solution, with consistent stirring at 800 rpm for 1 h. Then the pH of the solution was adjusted to 8, and the solution was stirred at 400 rpm for 20 min. After undisturbed at room temperature for 18 h, the solution was first sonicated and then centrifuged for 15 min at room temperature at 5600 rpm. The supernatant was gently removed, and the pellet in the centrifuge tube was sonicated for 3 min. The sedimented core–shell particles were redispersed three times in 15 mL of EtOH and twice with the same volume of ultrapure water.

For characterization, 50 μg AuNR (0.14 nM) was dissolved in 1 mL PBS buffer. 50 μg Ce6 (83.9 nM) was first dissolved in 100 μL DMSO and then diluted by PBS buffer to 1 ml. The PT materials were

first tested for their absorbance within NIR windows. 1 mL of each sample was transferred into quartz cuvettes, and the UV–vis–NIR absorption spectrophotometer (Agilent Cary 5000) was used to measure their absorption spectra between 500 and 1200 nm. The fluorescence of Ce6 was tested then through a 3D scan. 200 μL Ce6 solution was pipetted onto a 96-well plate and inserted into the plate reader. When the excitation wavelength varied from 450 to 550 nm, the emission fluorescence intensity between 600 and 800 nm was collected. The fluorescence peak can thus be utilized to evaluate the recruitment of Ce6.

Quantification of recruitment and efficiency for PT materials into GW26 CMs

To evaluate if the PT materials could be recruited by GW26 CMs, the peptide stock solution was pipetted into separate AuNR or Ce6 samples solubilized at a concentration of 50 μg/mL with a 1:9 (v/v) ratio to make CM suspensions. Fluorescence microscope images were collected for recruited Ce6, while high-resolution transmission electron microscopy (HRTEM, TEM JEOL 2100F) images were collected for recruited AuNR.

Then the recruitment efficiency for each material was measured using the characteristic absorption or fluorescence emission peak in the spectra of the corresponding PT materials obtained above. Before the measurements, the intensity of the peak for different PT materials (100 μL) under different concentrations was obtained on the spectrophotometer. According to Beer–Lambert law

$$A = \epsilon l c. \tag{2}$$

The intensity A has a linear relationship as a function of the solution concentration c within the low concentration range in the experiment. Thus, a reference A–c line could be obtained (Supplementary Figs. S7A and S7B). The suspension made above was centrifuged at 8000 rpm for Ce6 or 1000 rpm for AuNR for 10 min, making all CMs sediment at the bottom of the centrifuge tube. Then the absorption or fluorescence peak intensity of the supernatant was measured using a plate reader. The concentration of the supernatant was then derived from the reference curve. The concentration after (c_1) and before (c_2) recruitment was used to measure the recruitment efficiency η_r

$$\eta_r = \frac{c_2 - c_1}{c_2}. \tag{3}$$

Characterization of PT performance of recruited PT materials

1 mL of fresh CM suspension was pipetted into a 1.5 mL Eppendorf tube and put on a rack. The laser diode (Nanjing Zhixin Corp.) with a specific wavelength (680 or 808 nm) was placed vertically on the top of the tube mouth, with the exact location varying between 0.5 and 2 cm to achieve optimal irradiation. The power density of the laser was adjusted between 0.25 and 2 W/cm^2. The sample was irradiated for 5 min, during which an infrared camera (FLIR Systems Inc.) monitored the temperature of the samples every 0.5 min. After 5 min, the laser was turned off, and the temperature was recorded every 0.5 min for another 5 min. To test the reproducibility and the PT efficiency, this process was repeated five times.

The PT efficiency was then calculated using the general protocol commonly seen in previous research.[40] The efficiency η_h is defined as

$$\eta_h = \frac{hS\Delta T}{I(1 - 10^{-A})}, \tag{4}$$

where h refers to the heat absorption coefficient, S refers to the area exposed to light, ΔT refers to the variation of sample temperature (excluding the buffers, tubes, etc.), I refers to the power density of the laser, and A refers to the absorption of the sample. The value of T, I, and A can be obtained from the measurement, but the value of hS is obtained indirectly through the cooling process of PT materials. During this process, as the system has no thermal input, it satisfies

$$\Sigma(cm) \cdot T\mathrm{d}t = -hS\mathrm{d}T, \tag{5}$$

where c refers to heat capacity, m refers to mass, and t refers to time. By integrating it, we have

$$t = -\frac{\Sigma(cm)}{hS} \ln \frac{T - T_1}{T_0 - T_1}, \tag{6}$$

where T_0 represents the temperature before cooling and T_1 represents the temperature after cooling. Thus, hS can be derived from the slope of $t - \ln\frac{T-T_1}{T_0-T_1}$ graph (Supplementary Figs. S8A and S8B). Substituting the values of all variables into formula (3), the PT efficiency was obtained.

Delivery of PT materials into tumor cells and quantification of delivery efficiencies

CT26, HeLa, HCT116, and HT29 cancer cells were cultured in the CO_2 incubator (37.5 °C, 5% CO_2, Thermo Fisher Scientific Inc.). One day before delivery, 1×10^5 cells were suspended in media containing 90% plain media (RPMI/DMEM/McCoy) and 10% FBS and transferred to 35 cm^2 Petri dishes. After 24 h incubation, the cells were washed with PBS twice before their culture media was changed to 900 μL plain media and 100 μL fresh CMs suspension recruited either with AuNR or Ce6. Then the cells were incubated for another 4 h, removed from media, washed with PBS twice, and cultured in normal media (90% plain media, 10% FBS). Fluorescence and DIC images were collected for cells with and without CMs, Ce6, or AuNR, respectively, each day until the fifth day post-delivery, to observe the cellular uptake of PT material-recruited CMs.

Then the delivery efficiency of PT materials was evaluated. As for cells with Ce6 delivered, FACS was utilized to measure the efficiency: 2 days after delivery, around 5×10^5 cells were washed with PBS twice and treated with 0.25% trypsin-EDTA for 5 min to detach the cells from the wall of the dishes. The cell suspension was then centrifuged at 300 × g for 5 min, and the cell pellet was resuspended in 500 μL FACS buffer (95% PBS, 5% FBS) and transferred into a 5 mL round-bottom tube. The FACS analyzer (LSR Fortessa X20, BD Biosciences) then measured the fluorescence of the cell suspension at the excitation of 550 nm and emission of 650 nm and derived the delivery efficiency. As for cells with AuNR delivered, however, an alternative was applied as AuNR is not fluorescent: after the 4 h incubation post-delivery, the media containing CMs suspension was collected. 5% volume equivalent hydrochloric acid (1 M) was added to lower the pH, disassemble CMs, and release AuNR. Then the absorbance of the media at 808 nm was measured using a plate reader and divided by that of the group with culture media and CMs suspension but not used to culture any cell. The value represented the AuNR not entering the cells and was used to determine the delivery efficiency.

The cell viability after delivery of PT materials was quantified by MTT assay.[41] After delivery, the cells were incubated for 3 days. They were then washed by PBS for two times, and cultured in fresh media with 90% RPMI and 10% MTT (50 μM). After another 4 h incubation, 50% volume equivalent DMSO was added into each well to dissolve the precipitates. After 10 min incubation under room temperature, 100 μL of the solution was transferred into a 96-well plate, which was shaken for 5 min and inserted into the plate reader. The absorbance of the solution in the wells at 570 nm was measured. The cell viability was then calculated as

$$\eta = \frac{A_1 - A_2}{A_0 - A_2}, \tag{7}$$

where A_1 is the absorption of the experimental group, A_0 is the absorption of the control group with all live cells, and A_2 is the absorption of the control group with no cells.

Characterization of PT performance and cell cytotoxicity of recruited PT materials *in vitro*

Cancer cells were first incubated in 96-well plates with the initial density of $1 \times 10^4\,\mathrm{cm}^{-2}$. After 1 day incubation, recruited Ce6 or AuNR with different concentrations were delivered; for control groups, they were not treated with CMs or with free Ce6 or AuNR only. After another 1 day incubation, they were taken out and put on a horizontal surface. The laser diode (Nanjing Zhixin Group) with a specific wavelength (680 or 808 nm) was placed vertically on the top of the well with cells, with the exact location adjusted to achieve optimal irradiation by observing if the laser spot covered the whole well homogeneously. The power density of the laser was adjusted between 0.25 and 2 W/cm^2. Each well was irradiated for 5 min. After incubation for another 1 day, the MTT assay was utilized to quantify the viability of cells after laser treatment.

Then, Hoechst 33342 was used as a fluorescence dye to visualize the cell death after laser irradiation. The cells were separated from old media, washed twice by PBS, and added 1 mL Hoechst 33342 (100 ng/mL in PBS). After 15 min incubation at room temperature, the dye was discarded, and PBS was added to wash excessive dye twice before the addition of 1 mL plain RPMI. The cells were then observed with a fluorescence microscope at the emission of 460 nm when excited by 350 nm light for their morphology.

Characterization of co-delivery of PT materials and saporin and their cell cytotoxicity *in vitro*

Cancer cells were first incubated in 96-well plates with the initial density of $1 \times 10^4\,\mathrm{cm}^{-2}$. One day post-incubation, the media of cells was changed to 90 μL plain media and 10 μL fresh CMs suspension, prepared by pipetting 1 μL peptide stock solution into the mixture of 4.5 μL 100 μg/mL PT materials and 4.5 μL saporin solution with ideal concentration tested above. The cells were incubated for 4 h, and the media was changed to normal media (90% plain media, 10% FBS). After incubation for another 2 days, the MTT assay was utilized to determine the cell viability. Then the cells were put under a laser diode with a respective wavelength and irradiated under a 1 W/cm^2 laser for 5 min. After incubation for another 1 day, the MTT assay was utilized to determine the cell viability.

SUPPLEMENTARY MATERIAL

See the supplementary material for additional figures on peptide and PT materials characterization, cargo release characterization, PT performance of recruited PT materials, delivery of PT material-loaded CMs into cells, and *in vitro* PT performance.

ACKNOWLEDGMENTS

This research is supported by the National Research Foundation, Singapore, under its Competitive Research Programme (Award # NRF-CRP30-2023-0004). The authors gratefully acknowledge the Facility for Analysis, Characterisation, Testing and Simulation, Nanyang Technological University (FACTS), as well as the Microscope Facility, School of Biological Science, Nanyang Technological University for the support in utilization of imaging equipment. The author also thanks Professor Pu Kanyi from the School of Chemistry, Chemical Engineering and Biotechnology, Nanyang Technological University, Professor Xing Bengang, and Dr. Liu Songhan of School of Physical and Mathematical Sciences, Nanyang Technological University for their generous help on the PT study.

AUTHOR DECLARATIONS

Conflict of Interest

The authors have no conflicts to disclose.

Ethics Approval

Ethics approval is not required.

Author Contributions

Congxi Huang: Formal analysis (lead); Investigation (lead); Visualization (lead); Writing – original draft (equal). **Sushanth Gudlur:** Data curation (supporting); Investigation (supporting); Project administration (supporting); Validation (equal); Writing – review & editing (equal). **Syed Maricar:** Investigation (supporting). **Zilin Chen:** Investigation (supporting). **Anastasia Shebanova:** Investigation (supporting). **Yue Sun:** Investigation (supporting). **Valentin Saliba:** Investigation (supporting). **Cheng Xu:** Investigation (supporting). **Yiming Zou:** Investigation (supporting). **Jianghong Zhang:** Investigation (supporting). **Souhir Boujday:** Supervision (supporting); Validation (supporting). **Ali Miserez:** Conceptualization (lead); Funding acquisition (lead); Project administration (lead); Resources (lead); Supervision (lead); Writing – review & editing (equal).

DATA AVAILABILITY

The data that support the findings of this study are available within the article and its supplementary material.

REFERENCES

[1]S. Senapati, A. K. Mahanta, S. Kumar, and P. Maiti, Signal Transduction Targeted Ther. **3**(1), 7 (2018).
[2]G. Tiwari, R. Tiwari, B. Sriwastawa, L. Bhati, S. Pandey, P. Pandey, and S. K. Bannerjee, Int. J. Pharm. Invest. **2**(1), 2–11 (2012).
[3]L. Sercombe, T. Veerati, F. Moheimani, S. Y. Wu, A. K. Sood, and S. Hua, Front. Pharmacol. **6**, 286 (2015).

[4]E. Blanco, H. Shen, and M. Ferrari, Nat. Biotechnol. **33**(9), 941–951 (2015).
[5]S. Tahtinen, A.-J. Tong, P. Himmels, J. Oh, A. Paler-Martinez, L. Kim, S. Wichner, Y. Oei, M. McCarron, E. Freund, Z. Amir, C. de la Cruz, B. Haley, C. Blanchette, J. Schartner, W. Ye, M. Yadav, U. Sahin, L. Delamarre, and I. Mellman, Nat. Immunol. **23**(4), 532–542 (2022).
[6]S. Chatterjee, E. Kon, P. Sharma, and D. Peer, Proc. Natl. Acad. Sci. USA. **121**(11), e2307800120 (2024).
[7]M. M. Billingsley, N. Singh, P. Ravikumar, R. Zhang, C. H. June, and M. J. Mitchell, Nano Lett. **20**(3), 1578–1589 (2020).
[8]M. J. Mitchell, M. M. Billingsley, R. M. Haley, M. E. Wechsler, N. A. Peppas, and R. Langer, Nat. Rev. Drug Discov. **20**(2), 101–124 (2021).
[9]S. Chen, Q. Guo, and J. Yu, Aggregate **3**(6), e293 (2022).
[10]A. Shebanova, Q. Perrin, K. Zhu, S. Gudlur, Z. Chen, Y. Sun, C. Huang, Z. W. Lim, E. A. Mondarte, R. Sun, S. Lim, J. Yu, Y. Miao, A. Parikh, A. Ludwig, and A. Miserez, Adv. Sci. **11**(42), 2402652 (2024).
[11]A. Miserez, T. Schneberk, C. Sun, F. W. Zok, and J. H. Waite, Science **319**(5871), 1816–1819 (2008).
[12]Y. Tan, S. Hoon, P. A. Guerette, W. Wei, A. Ghadban, C. Hao, A. Miserez, and J. H. Waite, Nat. Chem. Biol. **11**(7), 488–495 (2015).
[13]B. Gabryelczyk, H. Cai, X. Shi, Y. Sun, P. J. M. Swinkels, S. Salentinig, K. Pervushin, and A. Miserez, Nat. Commun. **10**(1), 5465 (2019).
[14]Z. W. Lim, Y. Ping, and A. Miserez, Bioconjugate Chem. **29**(7), 2176–2180 (2018).
[15]Z. W. Lim, V. B. Varma, R. V. Ramanujan, and A. Miserez, Acta Biomater. **110**, 221–230 (2020).
[16]Y. Sun, S. Y. Lau, Z. W. Lim, S. C. Chang, F. Ghadessy, A. Partridge, and A. Miserez, Nat. Chem. **14**(3), 274–283 (2022).
[17]X. Li, J. F. Lovell, J. Yoon, and X. Chen, Nat. Rev. Clin. Oncol. **17**(11), 657–674 (2020).
[18]K. Ahmed, Y. Tabuchi, and T. Kondo, Apoptosis **20**(11), 1411–1419 (2015).
[19]C. Xu and K. Pu, Chem. Soc. Rev. **50**(2), 1111–1137 (2021).
[20]J. Li, W. Zhang, W. Ji, J. Wang, N. Wang, W. Wu, Q. Wu, X. Hou, W. Hu, and L. Li, J. Mater. Chem. B **9**(38), 7909–7926 (2021).
[21]R. Cavaliere, E. C. Ciocatto, B. C. Giovanella, C. Heidelberger, R. O. Johnson, M. Margottini, B. Mondovi, G. Moricca, and A. Rossi-Fanelli, Cancer **20**(9), 1351–1381 (1967).
[22]S. Sun, J. Chen, K. Jiang, Z. Tang, Y. Wang, Z. Li, C. Liu, A. Wu, and H. Lin, ACS Appl. Mater. Interfaces **11**(6), 5791–5803 (2019).
[23]X. Hu, H. Tian, W. Jiang, A. Song, Z. Li, and Y. Luan, Small **14**(52), 1802994 (2018).
[24]M. Nejabat, A. Samie, M. Ramezani, M. Alibolandi, K. Abnous, and S. M. Taghdisi, J. Controlled Release **354**, 221–242 (2023).
[25]M. L. Taylor, R. E. Wilson, Jr., K. D. Amrhein, and X. Huang, Bioengineering **9**(5), 200 (2022).
[26]S. Gudlur, G. Goyal, A. Pradhan, J. C. S. Ho, R. Srivastava, and B. Liedberg, Chem. Mater. **33**(12), 4558–4567 (2021).
[27]V. Pellas, J. Blanchard, C. Guibert, J.-M. Krafft, A. Miche, M. Salmain, and S. Boujday, ACS Appl. Nano Mater. **4**(9), 9842–9854 (2021).
[28]S. Maricar, S. Gudlur, and A. Miserez, Anal. Chem. **95**(26), 9924–9931 (2023).
[29]A. Hak, M. S. Ali, S. A. Sankaranarayanan, V. R. Shinde, and A. K. Rengan, ACS Appl. Bio Mater. **6**(2), 349–364 (2023).
[30]S. Link and M. A. El-Sayed, Int. Rev. Phys. Chem. **19**(3), 409–453 (2000).
[31]D. Pratap, Vikas, R. Gautam, A. K. Shaw, and S. Soni, Colloids Surf., A **635**, 128054 (2022).
[32]D. Pratap, R. K. Shah, S. Khandekar, and S. Soni, Appl. Nanosci. **12**(7), 2045–2058 (2022).
[33]B. He, X. Wang, H. Shi, W. Xiao, J. Zhang, B. Mu, Y. Mao, W. Wang, and Y. Wang, Integr. Cancer Ther. **12**(3), 264–270 (2013).
[34]J. Wei, J. Li, D. Sun, Q. Li, J. Ma, X. Chen, X. Zhu, and N. Zheng, Adv. Funct. Mater. **28**(17), 1706310 (2018).
[35]E. Glais, A. Maître, B. Viana, and C. Chanéac, Nanoscale Adv. **3**(10), 2862–2869 (2021).
[36]L. Polito, M. Bortolotti, D. Mercatelli, M. G. Battelli, and A. Bolognesi, Toxins **5**(10), 1698–1722 (2013).
[37]P. Varvarà, L. Tranchina, G. Cavallaro, and M. Licciardi, Appl. Sci. **10**(23), 8322 (2020).
[38]A. Casas, G. D. Venosa, T. Hasan, and B. Al, Curr. Med. Chem. **18**(16), 2486–2515 (2011).
[39]A. Dąbrowska, J. Mastalerz, B. Wilczyński, B. Osiecka, and A. Choromańska, Int. J. Mol. Sci. **25**(22), 12069 (2024).
[40]H. Chen, L. Shao, T. Ming, Z. Sun, C. Zhao, B. Yang, and J. Wang, Small **6**(20), 2272–2280 (2010).
[41]J. Van Meerloo, G. J. Kaspers, and J. Cloos, *Cell Sensitivity Assays: The MTT Assay* (Humana Press, 2011).